

A Bayesian Longitudinal Spatial Normative Model For Individualized Brain Deviation Mapping

Joshua T. Korley*

Department of Epidemiology & Biostatistics, University of South Carolina
jkorley@email.sc.edu

Abstract

Normative modeling enables individualized characterization of structural brain deviations by evaluating subjects against a reference population rather than a group average. Most existing implementations treat brain regions independently and remain cross-sectional, despite the availability of repeated neuroimaging measurements and the well-documented spatial organization of neuroanatomical variation. We propose a Bayesian longitudinal spatial normative model that jointly captures within-subject temporal dependence and spatially structured subject-specific deviations within a unified hierarchical framework. The individualized deviation map is treated as a latent spatial process with an explicit posterior distribution, yielding a principled Bayes estimator under squared error loss rather than an ad hoc residual summary. Across six simulation scenarios encompassing varying spatial dependence, nonlinear trajectories, irregular visit schedules, and missing follow-up, the proposed model consistently reduced deviation-map reconstruction error relative to cross-sectional and longitudinal non-spatial benchmarks while maintaining stable calibration. In an application to OASIS-3 structural MRI data, the model reduced RMSE by 54% and 45% relative to the two benchmarks. Regional deviation burden was concentrated in the temporal pole, entorhinal cortex, inferior temporal cortex, posterior cingulate, and parahippocampal cortex. Subject-level profiles revealed substantial heterogeneity in regional abnormality patterns, including marked multiregional deviation with preserved global cognitive scores.

Keywords: Hierarchical models, Neuroimaging, Conditional autoregressive prior, Repeated measures, Alzheimer’s disease, Posterior inference.

*This research received no specific grant from any funding agency in the public, commercial, or not-for-profit sectors. The author thanks colleagues and peers who provided helpful feedback and discussion during the development of this work. The author also acknowledges the OASIS-3 investigators and participants for making the neuroimaging and clinical data publicly available

1 Introduction

Neuroimaging studies have traditionally relied on population-average comparisons between diagnostic groups to characterize structural brain abnormalities. Although these approaches have produced important insights into neurological and psychiatric disease, they are less suited for describing heterogeneity at the individual level. Subjects with similar clinical diagnoses may exhibit markedly different spatial patterns of brain change, while substantial overlap often exists between patient and control populations. These limitations have motivated increasing interest in normative modeling approaches that estimate individualized deviations from a reference population rather than focusing exclusively on group-average effects (Marquand et al. 2016, Rutherford, Kia, Wolfers, Frazza, Zabihi, Dinga, Berthet, Worker, Verdi, Ruhe et al. 2022, Bethlehem et al. 2022).

Normative modeling shifts the focus of inference from group contrasts to individual deviation. The objective is to characterize a reference distribution for brain measures conditional on relevant covariates and to evaluate how each individual departs from this reference. This perspective parallels growth chart methodology, where observations are interpreted relative to expected trajectories. In neuroimaging, this formulation enables the study of heterogeneity within diagnostic categories and supports identification of subjects whose deviation patterns may reflect clinically meaningful or biologically distinct processes (Marquand et al. 2016, Rutherford, Kia, Wolfers, Frazza, Zabihi, Dinga, Berthet, Worker, Verdi, Ruhe et al. 2022, Frazza et al. 2021, Verdi et al. 2023).

Methodological developments have expanded this framework. Hierarchical Bayesian approaches improve robustness to site-specific variability and scanner effects (Kia et al. 2020). Flexible regression strategies extend applicability to non-Gaussian response distributions (Frazza et al. 2021). Large-scale studies demonstrate that normative trajectories can be estimated across the lifespan, yielding reference curves for structural brain phenotypes (Bethlehem et al. 2022). These contributions establish normative modeling as a core tool for individualized neuroimaging analysis.

Key structural features of neuroimaging data remain insufficiently addressed. One limitation concerns longitudinal structure. Repeated measurements are increasingly available, yet many implementations remain effectively cross-sectional or rely on sequential procedures that do not fully account for within-subject dependence. This leads to inefficient use of data and unstable deviation estimates when trajectories evolve over time ([Bucková et al. 2025](#)).

A second limitation concerns spatial dependence. Brain measurements exhibit structured relationships across anatomically and functionally related regions. Deviations from normative expectations frequently appear in spatially coherent patterns. Treating regions independently neglects this structure, reducing efficiency and distorting the geometry of estimated deviation maps. Spatial Bayesian models address related problems through structured priors that borrow strength across neighboring regions ([Huertas et al. 2017](#), [Mejia et al. 2022](#)). Spectral approaches extend spatial representation to higher resolution settings ([Sina et al. 2025](#)). These developments are rarely integrated within a normative modeling framework that targets individualized deviation in longitudinal data.

A third limitation concerns the role of deviation itself. In many applications, deviation is defined implicitly as a residual from a fitted model. When deviation is the primary scientific object, this representation is inadequate. In neurodegenerative and neurodevelopmental disorders, spatial configurations of deviation may encode information about disease processes that is not captured by marginal mean effects. A formulation that treats deviation as a structured latent quantity permits direct estimation and principled uncertainty quantification.

These limitations define a single inferential problem: estimation of subject-specific deviation maps that evolve over time and exhibit structured dependence across brain regions. Addressing this problem requires a model that captures longitudinal dynamics, spatial structure, and individual-level variation within a coherent probabilistic framework.

We develop a Bayesian longitudinal spatial normative model for repeated structural neuroimaging

measurements. The model combines a covariate-driven normative mean function, a subject-specific random intercept for repeated visits, and a spatially structured latent deviation process across brain regions. This formulation treats individualized deviation as the primary inferential target rather than as a secondary residual summary.

The paper makes three contributions. First, it introduces a region-level Bayesian normative model that jointly captures longitudinal dependence and spatially structured subject-specific deviation. Second, it characterizes the induced covariance structure and the posterior distribution of individualized spatial deviation maps under Gaussian assumptions. Third, it evaluates the model through simulation studies and an OASIS-3 structural MRI application, comparing it with independent cross-sectional and longitudinal non-spatial alternatives. This work addresses a gap in the literature. Prior research has established the importance of normative modeling for individualized inference ([Marquand et al. 2016](#), [Rutherford, Kia, Wolfers, Fraza, Zabihi, Dinga, Berthet, Worker, Verdi, Ruhe et al. 2022](#), [Fraza et al. 2021](#)), the role of hierarchical Bayesian methods for handling multi-site and heterogeneous data ([Kia et al. 2020](#)), and the value of spatial and longitudinal modeling when considered separately. In particular, longitudinal neuroimaging studies have emphasized subject-specific trajectories over time, while spatial Bayesian models have demonstrated the importance of borrowing information across anatomically related regions ([Mejia et al. 2022](#), [Sina et al. 2025](#)).

However, these developments have largely progressed in parallel. Existing spatial longitudinal models are primarily formulated for population-level inference, focusing on group differences or disease progression, and do not operate within a normative modeling framework that enables individualized deviation estimation. Conversely, current normative modeling approaches, including recent scalable Bayesian formulations, typically treat brain regions independently or do not explicitly incorporate subject-specific spatial structure.

A region-level framework that jointly models longitudinal trajectories and spatially structured

subject-specific deviations, while remaining interpretable and amenable to rigorous evaluation, remains limited. The proposed approach provides such a framework and supports individualized characterization of brain variation over time with quantified uncertainty.

The remainder of the paper is organized as follows. Section 2 presents the proposed Bayesian longitudinal spatial normative model, including the hierarchical formulation, posterior inference, and theoretical properties. Section 3 describes the simulation study and comparative evaluation under varying spatial and longitudinal data-generating settings. Section 4 applies the proposed framework to longitudinal structural MRI data from OASIS-3. Section 5 concludes with discussion, limitations, and directions for future research. Supplementary material provides additional theoretical derivations, simulation details, diagnostic analyses, and extended real-data results.

2 Methodology

2.1 Model formulation

We propose a Bayesian longitudinal spatial normative model for region-level structural MRI outcomes. Suppose there are n subjects indexed by $i = 1, \dots, n$, with subject i observed at visits $t = 1, \dots, T_i$. At each visit, measurements are recorded across R brain regions indexed by $r = 1, \dots, R$. Let Y_{itr} denote the structural measurement for subject i , visit t , and region r , and let $\mathbf{X}_{it} \in \mathbb{R}^p$ denote a visit-level covariate vector. The vector of regional measurements is written as $\mathbf{Y}_{it} = (Y_{it1}, \dots, Y_{itR})^\top$.

For each subject, visit, and region, the proposed model is

$$Y_{itr} = \mathbf{X}_{it}^\top \boldsymbol{\beta}_r + b_i + u_{ir} + \varepsilon_{itr}, \quad (1)$$

where $\boldsymbol{\beta}_r$ is a region-specific regression coefficient vector, b_i is a subject-specific random intercept, u_{ir} is a subject- and region-specific latent spatial deviation, and ε_{itr} is a residual error term. The

stochastic components are

$$b_i \stackrel{\text{iid}}{\sim} \mathcal{N}(0, \sigma_b^2), \quad \mathbf{u}_i = (u_{i1}, \dots, u_{iR})^\top \stackrel{\text{iid}}{\sim} \mathcal{N}(\mathbf{0}, \tau_u^2 \mathbf{Q}(\rho)^{-1}), \quad \varepsilon_{itr} \stackrel{\text{iid}}{\sim} \mathcal{N}(0, \sigma^2),$$

with mutual independence across the three latent components.

The spatial precision matrix is defined from a known region-level adjacency matrix. A convenient proper conditional autoregressive specification is

$$\mathbf{Q}(\rho) = \mathbf{D} - \rho \mathbf{W},$$

where \mathbf{W} is an $R \times R$ symmetric adjacency matrix, \mathbf{D} is diagonal with entries $D_{rr} = \sum_{s=1}^R W_{rs}$, and ρ lies in the admissible interval that ensures positive definiteness of $\mathbf{Q}(\rho)$ (Banerjee et al. 2003, Rue & Held 2005). This construction encourages anatomically related regions to share information while still allowing individualized regional heterogeneity.

In vector form, the model is

$$\mathbf{Y}_{it} = \mathbf{B}^\top \mathbf{X}_{it} + b_i \mathbf{1}_R + \mathbf{u}_i + \varepsilon_{it}, \quad (2)$$

where $\mathbf{B} = (\boldsymbol{\beta}_1, \dots, \boldsymbol{\beta}_R)$ is a $p \times R$ coefficient matrix whose r -th column corresponds to the region-specific coefficient vector $\boldsymbol{\beta}_r$, and $\varepsilon_{it} \sim \mathcal{N}(0, \sigma^2 \mathbf{I}_R)$. The normative mean function $\mathbf{X}_{it}^\top \boldsymbol{\beta}_r$ may be linear or may include spline basis terms for nonlinear age effects. In the simplest specification, \mathbf{X}_{it} includes an intercept, age, sex, and other relevant covariates. More flexible versions can replace age by a basis expansion without changing the hierarchical structure of the model.

2.2 Priors, prediction, and deviation scores

For the main Bayesian formulation, weakly informative Gaussian priors are assigned to the region-specific regression coefficients, $\boldsymbol{\beta}_r \stackrel{\text{iid}}{\sim} \mathcal{N}(\mathbf{0}, \sigma_\beta^2 \mathbf{I}_p)$, $r = 1, \dots, R$. Positive scale parameters may be assigned weakly informative half-Cauchy or exponential priors, depending on the

computational implementation: $\sigma_b > 0$, $\sigma > 0$, and $\tau_u > 0$. The spatial dependence parameter ρ is assigned a prior supported on the admissible interval of $\mathbf{Q}(\rho)$.

For a new or held-out observation (i, t, r) , the model yields a posterior predictive distribution. Let $\hat{\mu}_{itr} = \mathbb{E}(Y_{itr}^{\text{new}} \mid \mathcal{D})$, $\hat{v}_{itr} = \text{Var}(Y_{itr}^{\text{new}} \mid \mathcal{D})$, where \mathcal{D} denotes the observed data. Following the normative probability map construction of [Marquand et al. \(2016\)](#), we define the standardized deviation score $Z_{itr} = \frac{Y_{itr} - \hat{\mu}_{itr}}{\sqrt{\hat{v}_{itr}}}$.

Large negative values indicate unexpectedly small structural measurements relative to the normative reference model, while large positive values indicate unexpectedly large measurements. The vector $\mathbf{Z}_{it} = (Z_{it1}, \dots, Z_{itR})^\top$ is the individualized regional deviation map at visit t .

A subject-level summary of deviation burden may also be constructed by pooling absolute standardized deviations across visits and regions: $A_i^{(m)} = \frac{1}{m} \sum_{k=1}^m |Z_i|_{(k)}$, where $|Z_i|_{(1)} \geq \dots \geq |Z_i|_{(L_i)}$ are the ordered absolute deviation scores for subject i . This summary is useful for ranking subjects by overall deviation burden, but the primary inferential target remains the full regional deviation map.

2.3 Theoretical properties

We record the main properties needed for interpretation of the proposed model. Detailed proofs and additional theoretical results are given in the Supplementary Material.

Assumption 1 (Reference-model regularity). *The data arise from the hierarchical Gaussian model in (1), with $\mathbf{Q}(\rho)$ positive definite for the true value of ρ .*

Assumption 2 (Conditional independence). *Conditional on $(\mathbf{B}, b_i, \mathbf{u}_i)$, the residual vectors $\boldsymbol{\varepsilon}_{it}$ are independent across visits and subjects.*

Assumption 3 (Known adjacency). *The region-level adjacency matrix \mathbf{W} is fixed and known. The spatial precision matrix $\mathbf{Q}(\rho)$ is symmetric positive definite on the admissible parameter space*

of ρ .

Proposition 1 (Marginal mean and covariance). *Under model (1), the marginal mean of Y_{itr} is $\mathbb{E}(Y_{itr} | \mathbf{X}_{it}) = \mathbf{X}_{it}^\top \boldsymbol{\beta}_r$. For any two observations (i, t, r) and (j, s, ℓ) ,*

$$\text{Cov}(Y_{itr}, Y_{js\ell} | \mathbf{X}) = \mathbb{I}(i = j) \sigma_b^2 + \mathbb{I}(i = j) \tau_u^2 [\mathbf{Q}(\rho)^{-1}]_{r\ell} + \mathbb{I}(i = j, t = s, r = \ell) \sigma^2.$$

Proof. The result follows by subtracting the fixed mean in (1) and using independence of b_i , \mathbf{u}_i , and ε_{itr} . The random intercept contributes σ_b^2 to all observations from the same subject, the spatial deviation contributes $\tau_u^2 [\mathbf{Q}(\rho)^{-1}]_{r\ell}$ within subject across regions, and the residual contributes σ^2 only for the same subject, visit, and region. \square

Remark 1. Proposition 1 separates two sources of dependence. The random intercept induces subject-level dependence across all repeated measurements, while the spatial deviation process induces structured regional dependence within subject. Independent-region models do not capture this decomposition.

For a fixed subject i , define the residualized visit vector, $\tilde{\mathbf{Y}}_{it} = \mathbf{Y}_{it} - \mathbf{B}^\top \mathbf{X}_{it} - b_i \mathbf{1}_R$. Conditional on (\mathbf{B}, b_i) , model (2) implies $\tilde{\mathbf{Y}}_{it} = \mathbf{u}_i + \varepsilon_{it}$, $\varepsilon_{it} \stackrel{\text{iid}}{\sim} \mathcal{N}(\mathbf{0}, \sigma^2 \mathbf{I}_R)$.

Proposition 2 (Posterior distribution of subject-specific spatial deviations). *Fix subject i and suppose $(\mathbf{B}, b_i, \sigma^2, \tau_u^2, \rho)$ are known. Under (2), the conditional posterior distribution of \mathbf{u}_i given all visits of subject i is*

$$\mathbf{u}_i | \{\mathbf{Y}_{it}\}_{t=1}^{T_i}, \mathbf{B}, b_i, \sigma^2, \tau_u^2, \rho \sim \mathcal{N}(\mathbf{m}_i, \mathbf{S}_i), \quad (3)$$

where

$$\mathbf{S}_i = (\tau_u^{-2} \mathbf{Q}(\rho) + T_i \sigma^{-2} \mathbf{I}_R)^{-1}, \quad (4)$$

$$\mathbf{m}_i = \mathbf{S}_i \left(\sigma^{-2} \sum_{t=1}^{T_i} \tilde{\mathbf{Y}}_{it} \right). \quad (5)$$

Proof. The prior for \mathbf{u}_i is Gaussian with precision $\tau_u^{-2}\mathbf{Q}(\rho)$. The likelihood from the T_i residualized visits contributes precision $T_i\sigma^{-2}\mathbf{I}_R$ and linear term $\sigma^{-2}\sum_{t=1}^{T_i}\tilde{\mathbf{Y}}_{it}$. Completing the square yields (3)–(5). The full algebra is provided in the Supplementary Material. \square

Remark 2. Proposition 2 shows that the individualized deviation map is a posterior latent quantity, not an ad hoc residual image. The posterior covariance in (4) shows how repeated visits and spatial structure jointly influence shrinkage of subject-level deviation estimates.

Corollary 1 (Bayes estimator of the individualized deviation map). *Under squared error loss $L(\hat{\mathbf{u}}_i, \mathbf{u}_i) = \|\hat{\mathbf{u}}_i - \mathbf{u}_i\|_2^2$, the posterior mean $\hat{\mathbf{u}}_i^{\text{Bayes}} = \mathbb{E}(\mathbf{u}_i \mid \{\mathbf{Y}_{it}\}_{t=1}^{T_i}, \mathbf{B}, b_i, \sigma^2, \tau_u^2, \rho) = \mathbf{m}_i$ is the Bayes estimator of the subject-specific spatial deviation map.*

Remark 3. Corollary 1 gives the Bayesian interpretation of the individualized deviation map used throughout the paper. The posterior mean map is not only a smoothed residual summary; it is the Bayes estimator of the latent subject-specific spatial deviation process under squared error loss. A full decision-theoretic proof is provided in the Supplementary Material.

3 Simulation study

We evaluated the proposed model through six simulation scenarios representing distinct features of longitudinal neuroimaging data, including varying strengths of spatial dependence, unequal visit schedules, missing follow-up, and nonlinear mean trajectories. The primary goal was to assess whether joint modeling of repeated measurements and spatial dependence improves recovery of subject-specific deviation maps relative to independent cross-sectional and longitudinal non-spatial models.

Each simulated dataset consisted of region-level structural brain measurements observed over repeated visits. The data-generating mechanism matched the hierarchical structure of the proposed model so that the simulation estimand was the subject-specific spatial deviation map. For

each Monte Carlo replicate, we generated subject-level covariates, visit times, region-specific normative trajectories, subject random intercepts, spatial deviation maps, observation-level noise, and structured abnormality patterns in selected scenarios. Performance was summarized using estimation accuracy, deviation-map recovery, calibration, and abnormality-detection metrics.

3.1 Data-generating mechanism

Let $i = 1, \dots, n$ index subjects, $t = 1, \dots, T_i$ index visits, and $r = 1, \dots, R$ index brain regions. For each subject and visit, we generate a scalar age variable A_{it} and additional covariates collected in the vector \mathbf{X}_{it} . To maintain consistency with the main model, the synthetic response is generated according to

$$Y_{itr} = \mathbf{X}_{it}^\top \boldsymbol{\beta}_r + b_i + u_{ir} + \varepsilon_{itr}, \quad (6)$$

where:

$$\begin{aligned} b_i &\stackrel{\text{iid}}{\sim} \mathcal{N}(0, \sigma_b^2), \\ \mathbf{u}_i &= (u_{i1}, \dots, u_{iR})^\top \stackrel{\text{iid}}{\sim} \mathcal{N}(\mathbf{0}, \tau_u^2 \mathbf{Q}(\rho)^{-1}), \\ \varepsilon_{itr} &\stackrel{\text{iid}}{\sim} \mathcal{N}(0, \sigma^2). \end{aligned} \quad (7)$$

The precision matrix $\mathbf{Q}(\rho)$ is constructed from a fixed region-level adjacency matrix \mathbf{W} using

$$\mathbf{Q}(\rho) = \mathbf{D} - \rho \mathbf{W},$$

where \mathbf{D} is diagonal with entries $D_{rr} = \sum_{s=1}^R W_{rs}$. This is the standard proper conditional autoregressive construction used for structured areal spatial random effects (Rue & Held 2005, Banerjee et al. 2003, De Oliveira 2012). The use of a proper conditional autoregressive (CAR) form is particularly appropriate here because the simulation concerns region-indexed structural measurements rather than continuous Euclidean spatial fields.

3.1.1 Covariates and visit structure

In the baseline simulation design, each subject contributes between two and five visits. Let T_i be generated from a discrete distribution on $\{2, 3, 4, 5\}$, or fixed at a common value in scenarios intended to isolate other features of the design. Baseline age is generated as $A_{i1} \stackrel{\text{iid}}{\sim} \text{Uniform}(60, 85)$, and follow-up visit times are generated by adding irregular increments: $A_{it} = A_{i1} + \Delta_{it}$, $t = 2, \dots, T_i$, where Δ_{it} is generated from an increasing sequence with random perturbations to mimic unequally spaced visits. A binary sex indicator $S_i \stackrel{\text{iid}}{\sim} \text{Bernoulli}(0.5)$ is included as a time-invariant covariate. The resulting design vector takes the form $\mathbf{X}_{it} = (1, A_{it}, S_i)^\top$ in the baseline linear simulation. In nonlinear scenarios, the age term is replaced by a spline basis expansion.

3.1.2 Region-specific normative coefficients

For each region r , let $\boldsymbol{\beta}_r = (\beta_{0r}, \beta_{1r}, \beta_{2r})^\top$. The intercept β_{0r} represents the normative baseline level of region r , the coefficient β_{1r} represents the age effect, and β_{2r} represents the sex effect. To mimic heterogeneous regional trajectories, we generate region-specific coefficients as $\beta_{0r} \stackrel{\text{iid}}{\sim} \mathcal{N}(\mu_0, \sigma_0^2)$, $\beta_{1r} \stackrel{\text{iid}}{\sim} \mathcal{N}(\mu_1, \sigma_1^2)$, $\beta_{2r} \stackrel{\text{iid}}{\sim} \mathcal{N}(\mu_2, \sigma_2^2)$, with hyperparameters chosen so that the resulting trajectories resemble plausible variation in region-level brain structure. This random-coefficient construction is useful because it prevents the simulation from collapsing to a trivial common-trajectory setting and forces all competing models to estimate genuinely region-varying normative functions.

3.1.3 Subject-specific deviation maps

The vector \mathbf{u}_i in (7) represents the individualized latent deviation map for subject i . This component is central to the simulation because it is precisely the object that the proposed model is intended to recover. Spatial smoothness is controlled by the pair (τ_u^2, ρ) , where τ_u^2 governs the marginal scale and ρ governs the strength of adjacency-based dependence. When ρ is close to zero, deviations are weakly structured across regions. As ρ increases, neighboring regions become more

strongly correlated, which reflects the empirically motivated expectation that neuroanatomical abnormalities often appear in spatially coherent regional patterns rather than as independent region-wise perturbations (Huertas et al. 2017, Sina et al. 2025).

3.1.4 Residual variation

The residual term ε_{itr} captures within-visit measurement noise and unexplained variability. In the main simulation design, σ^2 is chosen to yield moderate signal-to-noise ratios. Additional scenarios vary σ^2 to assess robustness under low and high residual noise.

3.2 Abnormal subgroups and deviation signal injection

To evaluate abnormality-detection performance, we introduce a subgroup of non-reference subjects whose responses deviate systematically from the normative distribution. Let $G_i \in \{0, 1\}$ indicate whether subject i belongs to the abnormal subgroup. For $G_i = 0$, data are generated exactly from (6). For $G_i = 1$, we modify the data-generating process by adding a region-specific abnormality signal:

$$Y_{itr}^* = Y_{itr} + \delta_r, \tag{8}$$

where δ_r is nonzero only for a prespecified subset of abnormal regions $\mathcal{A} \subset \{1, \dots, R\}$. Several patterns of abnormality are considered:

1. Localized abnormality: only a small contiguous cluster of regions is shifted,
2. Diffuse abnormality: a larger distributed set of regions is shifted,
3. Mild abnormality: δ_r is small in magnitude,
4. Severe abnormality: δ_r is large in magnitude.

This setup directly evaluates whether the proposed posterior deviation scores can recover abnormal patterns when spatially structured signal is present. It also permits region-level sensitivity and

specificity calculations.

3.3 Simulation scenarios

The simulation considered six scenarios, each designed to isolate a feature commonly encountered in longitudinal neuroimaging data. In the no-spatial-dependence scenario, $\rho = 0$, so the regional deviation vector was uncorrelated across regions. This setting served as a negative control and assessed whether the proposed model imposed unnecessary cost when no spatial signal was present. In the moderate-spatial-dependence scenario, ρ was set to a moderate positive value, generating regional clustering in deviation maps. In the strong-spatial-dependence scenario, ρ was set to a larger value, inducing highly coherent regional deviation patterns and representing settings in which spatial borrowing should be most useful.

The remaining scenarios evaluated robustness to longitudinal and mean-structure complications. In the unequal-visit scenario, the number of visits varied across subjects, mimicking unbalanced longitudinal follow-up. In the missing-follow-up scenario, some later visits were removed under a missing-at-random mechanism depending on observed age and prior regional burden. In the nonlinear-trajectory scenario, the true age effect was nonlinear. For example, data could be generated as

$$Y_{itr} = \beta_{0r} + \beta_{1r}A_{it} + \beta_{2r}A_{it}^2 + \beta_{3r}S_i + b_i + u_{ir} + \varepsilon_{itr}.$$

In this nonlinear scenario, the coefficient vector is extended from the baseline linear form so that β_{2r} indexes the quadratic age effect and β_{3r} indexes the sex effect. This scenario evaluated the consequences of mean-function misspecification.

Structured abnormality patterns were introduced using the mechanism in (8). The same localized, diffuse, mild, and severe abnormality patterns were used across relevant scenarios, allowing region-level sensitivity, specificity, and deviation-map recovery to be evaluated against known truth.

3.4 Competing methods

The proposed model was compared with benchmark methods chosen to isolate the contributions of longitudinal and spatial structure. The benchmarks were not intended to exhaust all possible normative modeling approaches. Instead, they represented the main simplifications commonly used in neuroimaging applications: region-wise cross-sectional normative modeling, longitudinal normative modeling without spatial dependence, and the proposed joint longitudinal spatial formulation.

The first benchmark was an independent cross-sectional normative model. It ignored both repeated measurements and spatial dependence:

$$Y_{itr} = \mathbf{X}_{it}^\top \boldsymbol{\beta}_r + \varepsilon_{itr}.$$

All observations were treated as independent. This benchmark reflects the basic structure of region-wise normative modeling, in which separate predictive models are fit to individual brain regions or locations and subject-specific deviations are computed relative to the fitted normative distribution. This strategy has been central to neuroimaging normative modeling since its early use for individual-level inference in heterogeneous clinical cohorts (Marquand et al. 2016, 2019). More recent scalable Bayesian and distributional extensions, including hierarchical Bayesian regression and warped Bayesian linear regression, retain the same basic objective of estimating individualized deviations from a reference distribution while improving multi-site calibration, flexibility, and scalability (Kia et al. 2020, Frazza et al. 2021, Rutherford, Kia, Wolfers, Frazza, Zabihi, Dinga, Berthet, Worker, Verdi, Ruhe et al. 2022).

The second benchmark was a longitudinal non-spatial normative model. It accounted for repeated measurements through a subject-specific random intercept but ignored spatial dependence:

$$Y_{itr} = \mathbf{X}_{it}^\top \boldsymbol{\beta}_r + b_i + \varepsilon_{itr},$$

where $b_i \sim \mathcal{N}(0, \sigma_b^2)$. This model corresponds to the standard mixed-effects representation

for longitudinal data (Laird & Ware 1982). It is included because recent neuroimaging work has emphasized that normative modeling must move beyond single-occasion cross-sectional comparisons when the scientific question concerns within-person change, disease progression, or developmental trajectory (Gaiser et al. 2024, Bucková et al. 2025, Verdi et al. 2024). However, these longitudinal normative modeling strategies generally focus on temporal change or scanner harmonization and do not directly model a subject-specific spatial deviation process over brain regions. This benchmark therefore isolates the gain attributable to longitudinal structure alone.

The third method was the proposed Bayesian longitudinal spatial normative model:

$$Y_{itr} = \mathbf{X}_{it}^\top \boldsymbol{\beta}_r + b_i + u_{ir} + \varepsilon_{itr},$$

with $\mathbf{u}_i \sim \mathcal{N}(\mathbf{0}, \tau_u^2 \mathbf{Q}(\rho)^{-1})$. The spatial component is modeled as a Gaussian Markov random field, drawing on the conditional autoregressive and GMRF literature for spatially indexed data (Besag 1974, Rue & Held 2005, Banerjee et al. 2003). This formulation is motivated by the fact that structural brain deviations are often spatially coherent rather than independent across regions. Recent spatial normative modeling work has made a similar point at the level of high-resolution brain structure by showing that spatial representations can improve the characterization of individual deviation maps (Sina et al. 2025). The distinction in the present work is that spatial dependence is embedded directly within a longitudinal Bayesian hierarchical model, so the subject-specific deviation map is estimated jointly with repeated-measure dependence and normative covariate effects.

3.5 Performance measures and Monte Carlo implementation

The simulation used the same prior family as the estimation model. For regression coefficients, we assigned weakly informative Gaussian priors $\boldsymbol{\beta}_r \sim \mathcal{N}(\mathbf{0}, \sigma_\beta^2 \mathbf{I}_p)$. For the scale parameters σ , σ_b , and τ_u , we used half-Cauchy priors centered at zero with fixed scale hyperparameters. The choice of half-Cauchy priors follows the hierarchical modeling literature, where they have been

recommended as weakly informative defaults for variance components and as practical alternatives to inverse-Gamma priors in multilevel models (Gelman 2006, Polson & Scott 2012). For the spatial dependence parameter ρ , we used a prior supported on the admissible interval implied by $Q(\rho)$; a transformed Beta prior was used when a bounded support was required.

For each Monte Carlo replicate and each fitted method, performance was summarized using estimation accuracy, recovery of subject-specific deviation maps, calibration, abnormal-region detection, and predictive fit. Let μ_{itr}^{true} denote the true normative mean used in data generation, and let $\hat{\mu}_{itr}$ denote the fitted posterior predictive mean. Normative mean accuracy was evaluated using

$$\text{Bias} = \frac{1}{N_{\text{obs}}} \sum_{i,t,r} (\hat{\mu}_{itr} - \mu_{itr}^{\text{true}}), \quad \text{MSE} = \frac{1}{N_{\text{obs}}} \sum_{i,t,r} (\hat{\mu}_{itr} - \mu_{itr}^{\text{true}})^2.$$

Recovery of the subject-specific spatial deviation map was evaluated using

$$\text{Map-MSE} = \frac{1}{nR} \sum_{i=1}^n \|\hat{\mathbf{u}}_i - \mathbf{u}_i^{\text{true}}\|_2^2,$$

where $\mathbf{u}_i^{\text{true}}$ denotes the true latent deviation map and $\hat{\mathbf{u}}_i$ denotes its posterior mean estimate. This metric directly evaluates the primary object of methodological interest.

Calibration was assessed in two ways. First, for scalar targets, we calculated empirical coverage of nominal 95% posterior credible intervals for the normative mean and, where appropriate, for components of the subject-specific deviation map. Second, for observations generated from the reference subgroup, we evaluated whether the standardized deviation scores were centered near zero with variance close to one. Specifically, we summarized

$$\frac{1}{N_{\text{ref}}} \sum_{(i,t,r) \in \mathcal{N}} Z_{itr}, \quad \frac{1}{N_{\text{ref}} - 1} \sum_{(i,t,r) \in \mathcal{N}} (Z_{itr} - \bar{Z})^2.$$

We also recorded the empirical proportion of $|Z_{itr}| > 1.96$ in the reference subgroup as a practical tail-calibration check. Proper calibration is essential in normative modeling because deviation scores are interpreted probabilistically rather than only descriptively (Marquand et al. 2016, Rutherford, Kia, Wolfers, Frazz, Zabihi, Dinga, Berthet, Worker, Verdi, Ruhe et al. 2022).

For abnormal subjects, region-level detection was assessed by thresholding posterior deviation scores and comparing the flagged set with the true abnormal set \mathcal{A} . We reported sensitivity, specificity, positive predictive value, and the area under the receiver operating characteristic curve when continuous deviation scores were used. Predictive fit was also summarized using mean absolute error and mean standardized log-loss when useful, following the broader normative-modeling literature in which both central tendency and distributional fit are relevant (Sina et al. 2025).

For each scenario, M independent datasets were generated, with M chosen large enough to stabilize Monte Carlo summaries. Within each replicate, all competing methods were fit to the same generated dataset. Posterior inference was carried out using the same computational backend across Bayesian models, with common convergence diagnostics including trace inspection, \hat{R} , and effective sample size. Summary results were reported as Monte Carlo means together with Monte Carlo standard errors across replicates.

To avoid optimistic evaluation, abnormality-detection metrics were computed relative to the known generating truth rather than to the fitted model itself. Likewise, when the simulation used a distinct reference subgroup, fitting of the normative model was restricted to that subgroup before deviation scores were evaluated on held-out or abnormal subjects.

3.6 Simulation results

Each Monte Carlo dataset contained 120 subjects measured over 20 brain regions, with scenario-specific variation in spatial dependence, visit structure, missing follow-up, and mean-function form. The primary inferential target was recovery of the subject-specific deviation map. Results are reported in Tables 1–2 and Figures 1–2.

3.6.1 Estimation accuracy and deviation-map recovery

Table 1 and Figure 1 show that the Bayesian longitudinal spatial model achieved the lowest deviation-map mean squared error in every scenario. In the no-spatial-dependence setting, the proposed model produced a Map MSE of 0.352, compared with 0.690 for the longitudinal non-spatial model and 0.847 for the independent cross-sectional model. Thus, introducing spatial structure did not reduce performance when the generating mechanism contained no regional dependence.

The gains became larger when regional dependence was present. Under moderate spatial dependence, Map MSE decreased from 0.928 for the independent model and 0.718 for the longitudinal non-spatial model to 0.385 for the Bayesian longitudinal spatial model. Under strong spatial dependence, the corresponding values were 1.337, 0.930, and 0.604. Relative to the independent benchmark, the proposed model reduced map reconstruction error by approximately 55% under both moderate and strong spatial dependence. The same pattern appeared under unequal visit schedules, missing follow-up, and nonlinear mean trajectories. In the variable-visit scenario, the longitudinal non-spatial model had slightly smaller global MSE than the Bayesian longitudinal spatial model, 1.083 versus 1.093, but the proposed model had substantially lower Map MSE, 0.411 compared with 0.736. Under missing follow-up and nonlinear mean structure, the proposed model again produced the smallest Map MSE while maintaining stable global estimation accuracy. Across all scenarios, mean bias for the Bayesian longitudinal spatial model remained close to zero, ranging from 0.002 to 0.005. The independent model showed larger positive bias, ranging from 0.029 to 0.058, while the longitudinal non-spatial model ranged from 0.018 to 0.043.

Table 1: Simulation performance across the six data-generating scenarios. Lower values of mean squared error (MSE) and deviation-map reconstruction error (Map MSE) indicate improved recovery of the underlying latent deviation structure.

Simulation scenario	Model	Mean bias	MSE	Map MSE
No spatial dependence	Independent cross-sectional	0.031	1.145	0.847
	Longitudinal non-spatial	0.023	1.036	0.690
	Bayesian longitudinal spatial	0.002	0.887	0.352
Moderate spatial dependence	Independent cross-sectional	0.031	1.177	0.928
	Longitudinal non-spatial	0.022	1.027	0.718
	Bayesian longitudinal spatial	0.002	0.908	0.385
Strong spatial dependence	Independent cross-sectional	0.030	1.391	1.337
	Longitudinal non-spatial	0.018	1.074	0.930
	Bayesian longitudinal spatial	0.002	1.063	0.604
Variable visit schedule	Independent cross-sectional	0.030	1.392	1.136
	Longitudinal non-spatial	0.019	1.083	0.736
	Bayesian longitudinal spatial	0.002	1.093	0.411
Missing follow-up	Independent cross-sectional	0.029	1.385	1.119
	Longitudinal non-spatial	0.019	1.091	0.743
	Bayesian longitudinal spatial	0.002	1.086	0.410
Nonlinear mean structure	Independent cross-sectional	0.058	1.242	0.973
	Longitudinal non-spatial	0.043	1.088	0.758
	Bayesian longitudinal spatial	0.005	0.971	0.409

These results show that joint modeling of repeated measurements and regional dependence improves recovery of individualized deviation structure without sacrificing normative mean estimation accuracy. The pattern is consistent with the motivating premise that spatial structure is most useful

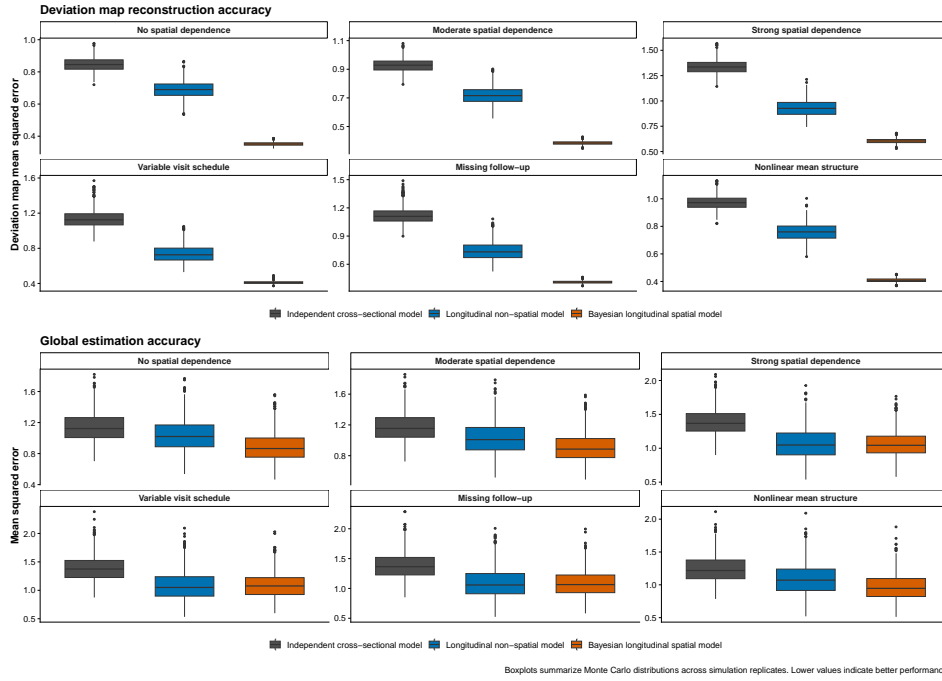


Figure 1: Estimation accuracy and deviation-map reconstruction across simulation scenarios. Boxplots summarize Monte Carlo distributions across simulation replicates. Lower values indicate better performance.

when subject-specific deviations are regionally coherent (Marquand et al. 2016, Rutherford, Kia, Wolfers, Fraza, Zabihi, Dinga, Berthet, Worker, Verdi, Ruhe et al. 2022, Sina et al. 2025).

3.6.2 Calibration of standardized deviation scores

Table 2 and Figure 2 summarize calibration of standardized deviation scores. The Bayesian longitudinal spatial model produced z-score means closest to zero across all scenarios, ranging from -0.004 to -0.001 . The independent model ranged from -0.046 to -0.022 , while the longitudinal non-spatial model ranged from -0.035 to -0.015 .

Table 2: Calibration performance across simulation scenarios. Target values are 0 for z-score mean, 1 for z-score variance, and 0.05 for tail probability.

Scenario	Model	<i>Z</i> mean	<i>Z</i> var.	Tail prob.
No spatial dependence	Independent cross-sectional	-0.025	0.981	0.044
	Longitudinal non-spatial	-0.020	0.920	0.037
	Bayesian longitudinal spatial	-0.002	0.966	0.046
Moderate spatial dependence	Independent cross-sectional	-0.025	0.981	0.044
	Longitudinal non-spatial	-0.018	0.904	0.036
	Bayesian longitudinal spatial	-0.002	0.966	0.046
Strong spatial dependence	Independent cross-sectional	-0.023	0.982	0.045
	Longitudinal non-spatial	-0.015	0.864	0.031
	Bayesian longitudinal spatial	-0.002	0.965	0.046
Variable visit schedule	Independent cross-sectional	-0.023	0.980	0.047
	Longitudinal non-spatial	-0.015	0.886	0.036
	Bayesian longitudinal spatial	-0.002	0.960	0.045
Missing follow-up	Independent cross-sectional	-0.022	0.981	0.047
	Longitudinal non-spatial	-0.015	0.889	0.036
	Bayesian longitudinal spatial	-0.001	0.964	0.046
Nonlinear mean structure	Independent cross-sectional	-0.046	0.965	0.042
	Longitudinal non-spatial	-0.035	0.890	0.034
	Bayesian longitudinal spatial	-0.004	0.955	0.044

The proposed model showed mild variance shrinkage, with z-score variance between 0.955 and 0.966. The independent model remained closer to the nominal target of 1, whereas the

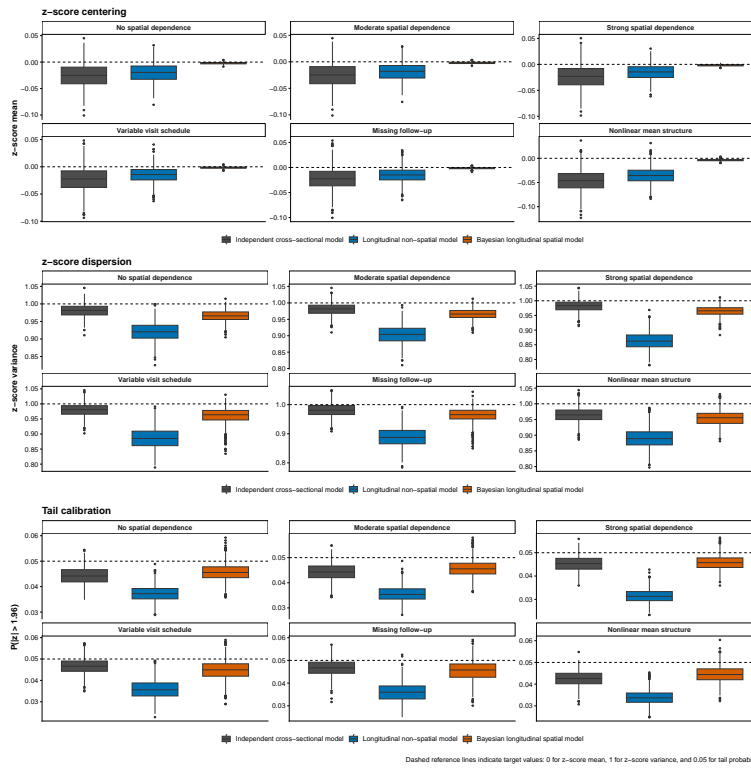


Figure 2: Calibration under varying spatial and longitudinal data-generating mechanisms. Dashed reference lines indicate target values: 0 for z-score mean, 1 for z-score variance, and 0.05 for tail probability.

longitudinal non-spatial model was more strongly under-dispersed, with variance ranging from 0.864 to 0.920. Tail calibration remained stable for the Bayesian longitudinal spatial model, with empirical probabilities of $|Z| > 1.96$ between 0.044 and 0.046, close to the nominal target of 0.05. The longitudinal non-spatial model produced smaller tail probabilities, especially under stronger spatial dependence.

The calibration results support the reconstruction findings. The proposed model produced substantially lower mean deviation-map error while preserving centered standardized scores and stable tail behavior. This operating behavior is important for individualized structural brain mapping, where the target is not only prediction but recovery of a spatial pattern of subject-level anatomical departure.

4 Application to OASIS-3 structural MRI

We applied the proposed model to longitudinal structural MRI data obtained from OASIS-3 (LaMontagne et al. 2019), a multimodal neuroimaging, clinical, cognitive, and biomarker resource for normal aging and Alzheimer disease. The OASIS-3 project includes repeated MRI sessions, FreeSurfer (Fischl et al. 2004) derived structural summaries, cognitive assessments, and clinical information collected through the Washington University Knight Alzheimer Disease Research Center. The application was designed to evaluate whether the proposed longitudinal spatial model improves subject-level normative deviation estimation in a real structural neuroimaging setting.

The analysis used FreeSurfer-derived regional measures from subjects with at least two MRI visits. We focused on a set of anatomically relevant cortical thickness and subcortical volume measures, including bilateral hippocampus, amygdala, entorhinal cortex, parahippocampal cortex, temporal pole, inferior temporal cortex, middle temporal cortex, posterior cingulate, and precuneus. Regional measures were standardized within region prior to modeling so that cortical thickness and volume features could be analyzed on a common scale. Age at MRI visit and FreeSurfer processing version were included as covariates. The model comparison used the same three-model structure as the simulation study: an independent cross-sectional model, a longitudinal non-spatial model with a subject random intercept, and the proposed Bayesian subject-specific spatial model.

The real-data analysis included 1,902 region-level observations for each selected region. The proposed Bayesian model was fit using four Markov chains with 1,000 warmup iterations and 1,000 post-warmup iterations per chain. The key posterior scale parameters were well identified. The residual standard deviation was estimated as 0.491, the subject-level random-intercept standard deviation as 0.517, the spatial deviation scale as 0.928, and the FreeSurfer-version scale as 0.305. The relatively large posterior mean of τ_u indicates substantial subject-specific spatial variation across brain regions after accounting for age, repeated observations, and processing version. This

is consistent with the motivating premise of the proposed model: individual structural brain deviations are not purely independent regional residuals, but have a structured spatial component.

4.1 Model comparison

The proposed Bayesian subject-specific spatial model provided the strongest fit among the three competing approaches (Table 3; Figure 3). The independent cross-sectional model had an RMSE of 0.926 and mean absolute deviation of 0.716. Adding a subject random intercept improved fit, reducing RMSE to 0.774 and mean absolute deviation to 0.597. The Bayesian subject-specific spatial model produced the largest improvement, reducing RMSE to 0.423 and mean absolute deviation to 0.306. These gains were not small changes in numerical fit. Relative to the independent cross-sectional model, the proposed model reduced RMSE by 54.3% and mean absolute deviation by 57.3%. Relative to the longitudinal non-spatial model, the proposed model reduced RMSE by 45.3% and mean absolute deviation by 48.7%.

Table 3: Model comparison in the OASIS-3 structural MRI application. Lower residual standard deviation, mean absolute deviation, and RMSE indicate improved model fit.

Model	Res. SD	MAD	RMSE	z-var	Tail prob.
Independent cross-sectional	0.926	0.716	0.926	1.000	0.0503
Longitudinal non-spatial	0.774	0.597	0.774	1.000	0.0482
Bayesian subject-specific spatial	0.423	0.306	0.423	0.743	0.0314

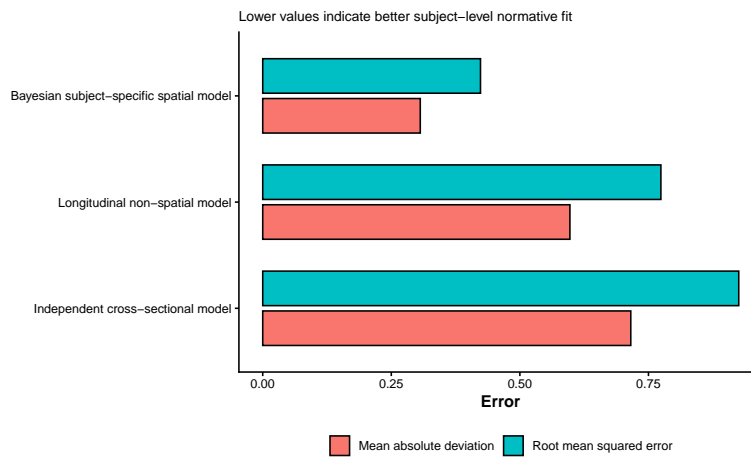


Figure 3: Model comparison in the OASIS-3 real-data application. The Bayesian subject-specific spatial model produced the lowest RMSE and mean absolute deviation, indicating improved subject-level normative fit relative to both benchmark models.

Thus, repeated-measure modeling improved the normative fit, but the largest gain came from modeling subject-specific spatial deviation across regions. This pattern agrees with the simulation results and supports the central methodological claim of the paper.

The standardized deviation summaries also showed an important difference between fit and calibration. The independent and longitudinal non-spatial models had z-score variances close to 1 by construction in the residual scale used for comparison, with tail probabilities of 0.0503 and 0.0482, respectively. The Bayesian spatial model had a smaller z-score variance of 0.743 and a tail probability of 0.0314. This under-dispersion reflects posterior shrinkage from the spatial hierarchical structure. In this application, the shrinkage is expected because the model borrows information across anatomically related regions and repeated visits. The result should therefore be interpreted as more conservative extreme-deviation calling, not as failure of the model. Supplementary Figures [S2-S5](#) provide additional calibration, QQ, and observed-versus-fitted diagnostics.

4.2 Posterior predictive assessment

Posterior predictive diagnostics were used to evaluate adequacy of the Bayesian longitudinal spatial normative model. Replicated datasets generated from the posterior predictive distribution showed close agreement with the observed distribution of standardized deviations, regional variability, and subject-level abnormality burden. Calibration histograms and QQ plots indicated that the posterior predictive standardized deviations remained approximately centered around the normative reference distribution while preserving anatomically structured variability across regions. Observed-versus-fitted comparisons further demonstrated that the proposed framework adequately captured both central tendency and subject-specific deviation structure across repeated visits. Additional posterior predictive diagnostics, including calibration histograms, QQ plots, and observed-versus-fitted comparisons, are provided in Supplementary Figures [S2-S5](#).

4.3 Regional and subject-level deviation patterns

The cortical atlas analysis showed that extreme standardized deviations were concentrated in temporolimbic and posterior association regions (Figure 4). A complementary map of posterior mean cortical standardized deviations is provided in Supplementary Figure [S1](#). The highest cortical tail probabilities occurred in the right temporal pole, left temporal pole, right entorhinal cortex, and left entorhinal cortex. These regions had tail probabilities of 0.0778, 0.0705, 0.0547, and 0.0515, respectively. Inferior temporal cortex, posterior cingulate, parahippocampal cortex, middle temporal cortex, and precuneus also appeared among the higher-burden regions.

This spatial pattern is biologically plausible. The entorhinal cortex, parahippocampal region, hippocampus, temporal pole, and inferior temporal cortex are closely related to memory and limbic-temporal networks affected early in Alzheimer-type neurodegeneration. Posterior cingulate and precuneus are also central regions in aging and Alzheimer disease research because of their

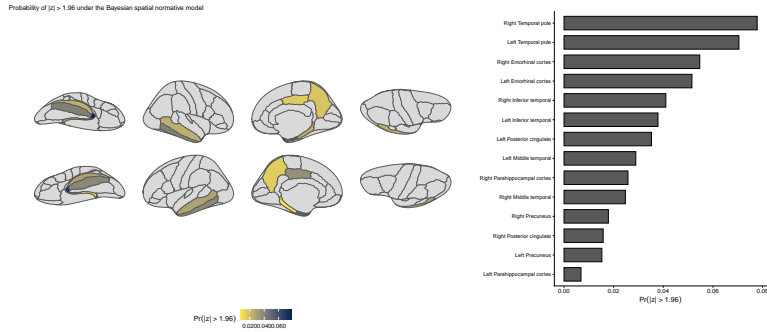


Figure 4: Cortical burden of extreme standardized deviations in the OASIS-3 application. The map displays $\Pr(|Z| > 1.96)$ across mapped cortical regions, with a ranked panel showing the corresponding region-level values. Highest burdens were observed in temporal pole and entorhinal regions, followed by inferior temporal, posterior cingulate, parahippocampal, middle temporal, and precuneus regions.

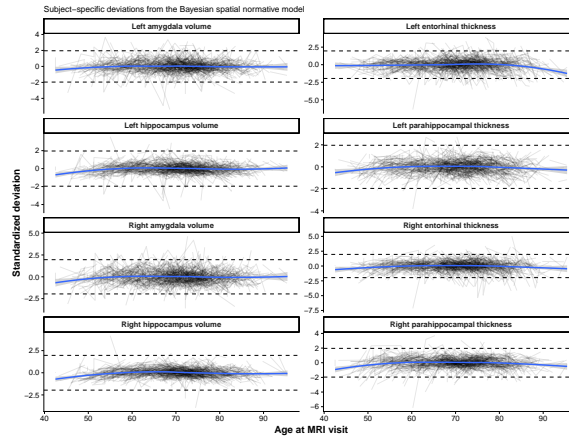


Figure 5: Longitudinal standardized deviation trajectories for selected structural regions. Gray lines represent subject-specific trajectories, blue curves summarize the average smoothed trajectory, and dashed horizontal lines denote ± 1.96 . Most subjects remained near the normative center, while a subset showed region-specific extreme deviations.

involvement in default-mode and memory-related networks. The model was not given diagnostic labels as the primary driver of these maps. The emergence of these regions from subject-level deviation estimates suggests that the proposed model is capturing meaningful anatomical variation

rather than only improving numerical fit.

Subcortical structures were not displayed in the Desikan-Killiany cortical atlas map, but the region-level table showed that left amygdala volume and right amygdala volume also had elevated abnormality burden, with tail probabilities of 0.0342 and 0.0331. The full ranked region summaries are provided in Supplementary Table S3. The longitudinal deviation trajectories

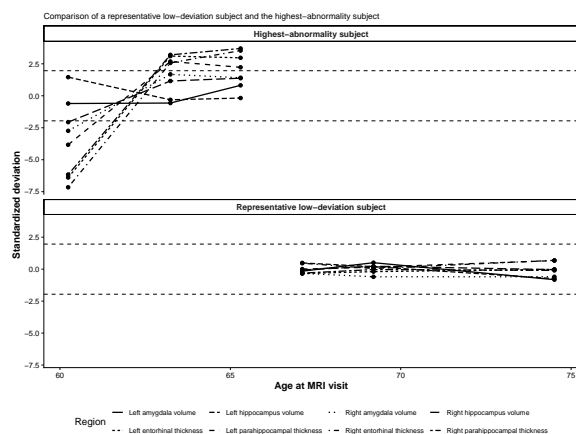


Figure 6: Illustrative subject-level deviation profiles. The upper panel shows the subject with the largest mean absolute standardized deviation, while the lower panel shows a representative low-deviation subject. Dashed horizontal lines denote ± 1.96 . The high-abnormality profile shows large and persistent deviations across several temporal and limbic regions, whereas the low-deviation profile remains close to the normative center.

provide a subject-level view of how structural deviations vary across age and region (Figure 5). Across the selected medial temporal and limbic regions, most trajectories remained close to zero, indicating that the fitted model preserved a stable normative center for the majority of observations. At the same time, a subset of subjects showed deviations outside the ± 1.96 reference bands, especially in hippocampal, amygdala, entorhinal, and parahippocampal measures. This is the desired behavior for a normative model: the population center remains stable while individual subjects can depart strongly from the expected structural profile.

The smoothed trajectories were generally near zero across age, with modest curvature in several regions. This suggests that the model adjusted for age-related mean trends while still allowing subject-specific departures from the fitted normative surface. The full calibration and observed-versus-fitted diagnostics are reported in Supplementary Figures [S2-S3](#).

The subject-level case study illustrates how the proposed model can separate a stable low-deviation profile from a highly abnormal regional deviation profile (Figure [6](#)). The highest-abnormality subject, OAS30303, had 57 observations across three MRI visits, mean absolute standardized deviation 3.97, maximum absolute deviation 10.5, and 77.2% of observations exceeding $|Z| > 1.96$. The subject had mean MMSE 29.7 and mean CDR total score 0, indicating that the structural deviation profile was not simply a reflection of severe measured cognitive impairment at the available visits.

This example is important because it shows the scientific value of individualized normative modeling. A subject may have strong multiregional structural deviation even when global cognitive summaries remain within a clinically normal or minimally impaired range. The proposed model therefore provides a way to identify spatially coherent anatomical deviation patterns that may be hidden by group-level summaries or by cognitive status alone. The representative low-deviation subject remained close to the normative center across selected regions and visits, demonstrating the contrast between stable normative aging and marked subject-level anatomical departure. The full distribution of subject-level abnormality burden is shown in Supplementary Figure [S6](#), and full subject summaries are provided in Supplementary Table [S2](#).

5 Discussion

In this paper, we developed a Bayesian longitudinal spatial normative model for individualized brain deviation mapping from repeated structural neuroimaging measurements. The framework was

motivated by a limitation of many existing normative approaches: individualized deviation is often treated implicitly as a residual after estimation of a normative mean model. In longitudinal neuroimaging settings, deviation itself may exhibit persistent spatial organization across anatomically related regions and repeated visits. The proposed formulation addresses this directly by modeling individualized deviation as a subject-specific latent spatial process within a longitudinal Bayesian framework.

The theoretical results provide the individualized deviation map with a formal Bayesian interpretation. Conditional on model parameters, the posterior distribution of the latent spatial deviation vector combines information across repeated visits and neighboring brain regions. Under squared error loss, the posterior mean is the Bayes estimator of the individualized deviation map. The resulting map is therefore not an ad hoc smoothed residual image but a posterior estimand with an explicit covariance structure and principled uncertainty quantification. This distinction is central to the methodological contribution of the paper.

Simulation results confirmed that jointly modeling longitudinal and spatial structure consistently improved deviation-map reconstruction relative to both benchmarks, with the strongest gains under moderate and strong spatial dependence. Critically, the model remained stable when spatial dependence was weak, and maintained well-calibrated deviation scores across all scenarios. In normative modeling, deviation scores are interpreted relative to a covariate-adjusted reference distribution rather than as ordinary prediction residuals (Marquand et al. 2016, Rutherford, Kia, Wolfers, Frazz, Zabihi, Dinga, Berthet, Worker, Verdi, Ruhe et al. 2022, Rutherford, Barkema, Tso, Sripada, Beckmann, Ruhe & Marquand 2022). The benchmark comparisons further showed that subject random intercepts alone cannot represent how deviations are distributed across brain regions: longitudinal dependence is necessary but insufficient when the inferential target is the regional organization of individualized anatomical departure.

In the OASIS-3 application, the largest improvement occurred after introducing the subject-specific spatial deviation process. The posterior mean of the spatial deviation scale exceeded the residual scale, indicating that structured regional heterogeneity is an important component of subject-level variation. The Bayesian spatial model produced lower z-score variance and fewer extreme deviations than the benchmarks, reflecting posterior shrinkage from borrowing information across anatomically related regions and repeated visits. Such shrinkage may be desirable in individualized neuroimaging analysis because isolated extreme residuals may reflect measurement instability rather than coherent anatomical abnormality. Under the proposed framework, observations are flagged as extreme only after accounting for age, repeated measurements, processing version, and regional dependence.

The proposed framework is related to several existing directions in normative modeling and Bayesian neuroimaging but addresses a different inferential objective. Normative modeling established covariate-adjusted reference distributions for individualized inference ([Marquand et al. 2016](#), [Rutherford, Kia, Wolfers, Fraza, Zabihi, Dinga, Berthet, Worker, Verdi, Ruhe et al. 2022](#)). Hierarchical Bayesian extensions improved multi-site calibration ([Kia et al. 2020](#), [Bayer et al. 2022](#)). Distributional and warped approaches extended the framework beyond Gaussian assumptions ([Fraza et al. 2021](#)). Bayesian spatial neuroimaging models demonstrated structured borrowing across brain regions ([Huertas et al. 2017](#), [Mejia et al. 2022](#)), and recent spectral normative models showed that spatial representations support high-resolution deviation mapping ([Sina et al. 2025](#)). The present work is complementary to these developments. Its emphasis is joint Bayesian estimation of longitudinal dependence and subject-specific spatial deviation, with individualized deviation treated as the primary latent inferential target rather than spectral reconstruction or atlas-free spatial querying.

The regional findings in OASIS-3 were anatomically plausible. The largest extreme-deviation burdens were observed in the temporal pole, entorhinal cortex, inferior temporal cortex, posterior

cingulate, parahippocampal cortex, middle temporal cortex, precuneus, and amygdala. These regions are closely associated with medial temporal memory systems and posterior association networks implicated in Alzheimer-related neurodegeneration ([Dickerson et al. 2009](#), [Bakkour et al. 2009](#), [Verdi et al. 2021, 2023](#)). The model was not developed as a diagnostic classifier and these findings should not be interpreted as validated disease biomarkers. After adjustment for age, repeated measurements, processing version, and spatial dependence, the proposed framework recovered coherent deviation patterns in regions where neurodegenerative structural variation is biologically plausible. At the subject level, the highest-abnormality case exhibited widespread multiregional deviation despite relatively preserved cognitive summaries, illustrating that structural deviation and global cognitive measures may not align at a single time point ([Verdi et al. 2021, 2023](#)).

The study has limitations. The OASIS-3 analysis used selected cortical and subcortical regions rather than vertex-wise or voxel-wise representations, limiting spatial resolution. The adjacency structure was anatomically specified rather than estimated from the data; future work could compare anatomical, connectivity-based, and data-adaptive spatial structures. The present formulation assumes Gaussian residual variation, and structural neuroimaging measurements may exhibit skewness or heavy tails, motivating extensions using warped or more flexible likelihood formulations ([Fraza et al. 2021](#)). Extension to vertex-wise settings would require sparse precision methods, reduced-rank spatial representations, or approximate Bayesian inference. Future work should also evaluate whether individualized deviation burden predicts longitudinal cognitive decline, biomarker progression, or treatment response across external cohorts.

The proposed model extends normative modeling to settings where individualized anatomical deviation evolves over time and exhibits structured dependence across brain regions. Individualized deviation is represented as a structured latent process with an explicit posterior distribution, linking normative modeling ([Marquand et al. 2016](#), [Rutherford](#), [Barkema](#), [Tso](#), [Sripada](#), [Beckmann](#), [Ruhe](#)

& Marquand 2022, Rutherford, Kia, Wolfers, Fraza, Zabihi, Dinga, Berthet, Worker, Verdi, Ruhe et al. 2022, Verdi et al. 2021, 2023) to longitudinal mixed-effects methodology and Bayesian spatial modeling (Huertas et al. 2017, Mejia et al. 2022, Sina et al. 2025). The results support longitudinal spatial normative modeling for individualized neuroimaging analysis when the primary scientific interest is the regional organization of anatomical departure rather than population-average trajectories.

Disclosure statement

The author declares no conflicts of interest exist.

Data Availability Statement

The OASIS-3 dataset used in this study is publicly available through the OASIS Brains project upon approved data use agreement at <https://www.oasis-brains.org>. All statistical analyses were conducted in R. Code supporting the simulation study, Bayesian model fitting, posterior inference, and figure generation is available through an archived repository: <https://doi.org/10.5281/zenodo.20154009>

SUPPLEMENTARY MATERIAL

For

A Bayesian Longitudinal Spatial Normative Model

For Individualized Brain Deviation Mapping

S1 Additional model details

This supplement provides technical and computational material supporting the main manuscript. Section S1 records additional modeling details and notation. Section S2 presents theoretical derivations and proofs that complement the primary methodological development in the main text. Section S3 describes the simulation implementation in greater detail, including construction of the spatial dependence structure and generation of individualized abnormality patterns. Section S4 reports additional simulation summaries and calibration diagnostics. Section S5 provides extended analyses for the OASIS-3 structural neuroimaging application, including preprocessing details, posterior diagnostics, supplementary cortical maps, and additional subject-level analyses. Section S6 summarizes computational implementation details and software settings.

The proposed Bayesian longitudinal spatial normative model is

$$Y_{itr} = \mathbf{X}_{it}^\top \boldsymbol{\beta}_r + b_i + u_{ir} + \varepsilon_{itr},$$

where Y_{itr} denotes the structural neuroimaging measurement for subject i , visit t , and region r , \mathbf{X}_{it} contains visit-level covariates, b_i is a subject-specific random intercept, and u_{ir} represents the latent subject-specific spatial deviation process. The residual errors satisfy

$$\varepsilon_{itr} \sim \mathcal{N}(0, \sigma^2).$$

The subject-level random intercepts are modeled as

$$b_i \sim \mathcal{N}(0, \sigma_b^2),$$

and the regional spatial deviation vectors are assigned the prior

$$\mathbf{u}_i \sim \mathcal{N}(\mathbf{0}, \tau_u^2 \mathbf{Q}(\rho)^{-1}),$$

where $\mathbf{Q}(\rho)$ is a spatial precision matrix constructed from a region-level adjacency structure. The primary inferential target is the individualized deviation map \mathbf{u}_i , which quantifies how each subject deviates from the expected normative trajectory after accounting for age, repeated measurements, and anatomical dependence across regions.

S2 Additional theoretical results and proofs

S2.1 Nested submodel structure

Supplementary Proposition S1 (Nested submodels). *Consider the hierarchical model*

$$Y_{itr} = \mathbf{X}_{it}^\top \boldsymbol{\beta}_r + b_i + u_{ir} + \varepsilon_{itr}.$$

Several commonly used neuroimaging normative models arise as special cases under restrictions on the variance components.

1. *If $\tau_u^2 = 0$, the model reduces to a longitudinal non-spatial normative model.*
2. *If $\sigma_b^2 = 0$, dependence across regions is induced only through the spatial deviation process.*
3. *If $\tau_u^2 = 0$, $\sigma_b^2 = 0$, and $T_i = 1$ for all subjects, the model reduces to an independent cross-sectional regional model.*
4. *If the regional mean functions in part (3) are estimated separately using nonparametric predictive models, the resulting formulation corresponds to conventional region-wise normative modeling approaches commonly used in neuroimaging studies.*

Proof. For part (1), setting $\tau_u^2 = 0$ implies

$$u_{ir} = 0$$

almost surely for all regions. The model simplifies to

$$Y_{itr} = \mathbf{X}_{it}^\top \boldsymbol{\beta}_r + b_i + \varepsilon_{itr},$$

which retains within-subject longitudinal dependence through b_i but removes spatial dependence across regions.

For part (2), setting $\sigma_b^2 = 0$ implies

$$b_i = 0$$

almost surely. The model becomes

$$Y_{itr} = \mathbf{X}_{it}^\top \boldsymbol{\beta}_r + u_{ir} + \varepsilon_{itr}.$$

In this setting, the only source of dependence across regions arises from the covariance structure of the spatial deviation vector \mathbf{u}_i .

For part (3), if $\tau_u^2 = 0$, $\sigma_b^2 = 0$, and $T_i = 1$, then

$$Y_{i1r} = \mathbf{X}_{i1}^\top \boldsymbol{\beta}_r + \varepsilon_{i1r}.$$

Since the residual terms are independent across regions, each region is modeled independently without spatial or longitudinal borrowing.

Part (4) follows by replacing the parametric regional mean structure with separate nonparametric predictive functions estimated independently for each region. This recovers the structure used in many existing region-wise neuroimaging normative models. \square

S2.2 Posterior distribution of the spatial deviation map

For subject i , define the residualized observation vector

$$\tilde{\mathbf{Y}}_{it} = \mathbf{Y}_{it} - \mathbf{B}^\top \mathbf{X}_{it} - b_i \mathbf{1}_R,$$

where $\mathbf{1}_R$ denotes an R -dimensional vector of ones.

Conditional on \mathbf{u}_i ,

$$\tilde{\mathbf{Y}}_{it} = \mathbf{u}_i + \boldsymbol{\varepsilon}_{it},$$

with

$$\boldsymbol{\varepsilon}_{it} \sim \mathcal{N}(\mathbf{0}, \sigma^2 \mathbf{I}_R).$$

The prior density of \mathbf{u}_i is proportional to

$$\exp \left\{ -\frac{1}{2\tau_u^2} \mathbf{u}_i^\top \mathbf{Q}(\rho) \mathbf{u}_i \right\}.$$

The likelihood contribution from all visits of subject i is proportional to

$$\prod_{t=1}^{T_i} \exp \left\{ -\frac{1}{2\sigma^2} (\tilde{\mathbf{Y}}_{it} - \mathbf{u}_i)^\top (\tilde{\mathbf{Y}}_{it} - \mathbf{u}_i) \right\}.$$

Combining the prior and likelihood gives the posterior kernel

$$\exp \left[-\frac{1}{2\tau_u^2} \mathbf{u}_i^\top \mathbf{Q}(\rho) \mathbf{u}_i - \frac{1}{2\sigma^2} \sum_{t=1}^{T_i} (\tilde{\mathbf{Y}}_{it} - \mathbf{u}_i)^\top (\tilde{\mathbf{Y}}_{it} - \mathbf{u}_i) \right].$$

Expanding the likelihood term,

$$\sum_{t=1}^{T_i} (\tilde{\mathbf{Y}}_{it} - \mathbf{u}_i)^\top (\tilde{\mathbf{Y}}_{it} - \mathbf{u}_i) = \sum_{t=1}^{T_i} \tilde{\mathbf{Y}}_{it}^\top \tilde{\mathbf{Y}}_{it} - 2\mathbf{u}_i^\top \sum_{t=1}^{T_i} \tilde{\mathbf{Y}}_{it} + T_i \mathbf{u}_i^\top \mathbf{u}_i.$$

Dropping terms independent of \mathbf{u}_i yields

$$\exp \left\{ -\frac{1}{2} \mathbf{u}_i^\top \left(\tau_u^{-2} \mathbf{Q}(\rho) + T_i \sigma^{-2} \mathbf{I}_R \right) \mathbf{u}_i + \mathbf{u}_i^\top \left(\sigma^{-2} \sum_{t=1}^{T_i} \tilde{\mathbf{Y}}_{it} \right) \right\}.$$

Completing the square gives

$$\mathbf{u}_i \mid \{\mathbf{Y}_{it}\}_{t=1}^{T_i}, \mathbf{B}, b_i, \sigma^2, \tau_u^2, \rho \sim \mathcal{N}(\mathbf{m}_i, \mathbf{S}_i),$$

where

$$\mathbf{S}_i = (\tau_u^{-2} \mathbf{Q}(\rho) + T_i \sigma^{-2} \mathbf{I}_R)^{-1},$$

and

$$\mathbf{m}_i = \mathbf{S}_i \left(\sigma^{-2} \sum_{t=1}^{T_i} \tilde{\mathbf{Y}}_{it} \right).$$

The posterior mean \mathbf{m}_i therefore combines subject-specific longitudinal information with anatomically structured spatial borrowing across regions.

S2.3 Posterior predictive distribution

Supplementary Proposition S2 (Posterior predictive distribution). *For a future visit t^* of subject i with covariates \mathbf{X}_{it^*} ,*

$$\mathbf{Y}_{it^*}^{\text{new}} \mid \{\mathbf{Y}_{it}\}_{t=1}^{T_i} \sim \mathcal{N}(\mathbf{B}^\top \mathbf{X}_{it^*} + b_i \mathbf{1}_R + \mathbf{m}_i, \mathbf{S}_i + \sigma^2 \mathbf{I}_R).$$

Proof. The predictive model satisfies

$$\mathbf{Y}_{it^*}^{\text{new}} = \mathbf{B}^\top \mathbf{X}_{it^*} + b_i \mathbf{1}_R + \mathbf{u}_i + \boldsymbol{\varepsilon}_{it^*}^{\text{new}},$$

where

$$\boldsymbol{\varepsilon}_{it^*}^{\text{new}} \sim \mathcal{N}(\mathbf{0}, \sigma^2 \mathbf{I}_R)$$

and is conditionally independent of \mathbf{u}_i .

Since

$$\mathbf{u}_i \mid \dots \sim \mathcal{N}(\mathbf{m}_i, \mathbf{S}_i),$$

the sum

$$\mathbf{u}_i + \boldsymbol{\varepsilon}_{it^*}^{\text{new}}$$

is Gaussian with mean \mathbf{m}_i and covariance

$$\mathbf{S}_i + \sigma^2 \mathbf{I}_R.$$

Adding the deterministic mean component gives the stated predictive distribution. □

S2.4 Oracle standardization

Supplementary Proposition S3 (Oracle standardization). *Assume the normative model is correctly specified and that all model parameters are known. Let*

$$\mu_{itr} = \mathbb{E}(Y_{itr} \mid \text{history}),$$

and

$$v_{itr} = \text{Var}(Y_{itr} \mid \text{history}).$$

Then

$$Z_{itr}^\circ = \frac{Y_{itr} - \mu_{itr}}{\sqrt{v_{itr}}} \sim \mathcal{N}(0, 1).$$

Proof. Under correct model specification,

$$Y_{itr} \mid \text{history} \sim \mathcal{N}(\mu_{itr}, v_{itr}).$$

Subtracting the true predictive mean and dividing by the true predictive standard deviation standardizes the Gaussian variable. Therefore,

$$\frac{Y_{itr} - \mu_{itr}}{\sqrt{v_{itr}}} \sim \mathcal{N}(0, 1).$$

□

S2.5 Bayes optimality of spatial borrowing

A principal motivation for introducing \mathbf{u}_i with structured covariance is that spatial borrowing should improve estimation of individualized deviation maps when the regional dependence model is correctly specified. This can be stated formally.

Supplementary Proposition S4 (Posterior mean as Bayes-optimal deviation estimator). *Fix subject i and suppose the hierarchical model is correctly specified. Under squared error loss*

$$L(\hat{\mathbf{u}}_i, \mathbf{u}_i) = \|\hat{\mathbf{u}}_i - \mathbf{u}_i\|_2^2,$$

the posterior mean

$$\hat{\mathbf{u}}_i^{\text{Bayes}} = \mathbb{E}(\mathbf{u}_i \mid \{\mathbf{Y}_{it}\}_{t=1}^{T_i}, \mathbf{B}, b_i, \sigma^2, \tau_u^2, \rho) = \mathbf{m}_i$$

minimizes posterior expected loss over all measurable estimators of \mathbf{u}_i based on subject i 's data.

Proof. Let $\hat{\mathbf{u}}_i$ be any measurable estimator based on the observed data for subject i . Conditional on the observed data and model parameters, the posterior expected loss is

$$R(\hat{\mathbf{u}}_i) = \mathbb{E}[\|\hat{\mathbf{u}}_i - \mathbf{u}_i\|_2^2 \mid \{\mathbf{Y}_{it}\}_{t=1}^{T_i}, \mathbf{B}, b_i, \sigma^2, \tau_u^2, \rho].$$

Let $\mathbf{m}_i = \mathbb{E}(\mathbf{u}_i \mid \{\mathbf{Y}_{it}\}_{t=1}^{T_i}, \mathbf{B}, b_i, \sigma^2, \tau_u^2, \rho)$. Expanding the squared loss around \mathbf{m}_i gives

$$\begin{aligned} \|\hat{\mathbf{u}}_i - \mathbf{u}_i\|_2^2 &= \|\hat{\mathbf{u}}_i - \mathbf{m}_i + \mathbf{m}_i - \mathbf{u}_i\|_2^2 \\ &= \|\hat{\mathbf{u}}_i - \mathbf{m}_i\|_2^2 + \|\mathbf{m}_i - \mathbf{u}_i\|_2^2 + 2(\hat{\mathbf{u}}_i - \mathbf{m}_i)^\top (\mathbf{m}_i - \mathbf{u}_i). \end{aligned}$$

Taking posterior expectation conditional on the observed data yields

$$\begin{aligned} R(\hat{\mathbf{u}}_i) &= \|\hat{\mathbf{u}}_i - \mathbf{m}_i\|_2^2 + \mathbb{E}[\|\mathbf{m}_i - \mathbf{u}_i\|_2^2 \mid \{\mathbf{Y}_{it}\}_{t=1}^{T_i}, \mathbf{B}, b_i, \sigma^2, \tau_u^2, \rho] \\ &\quad + 2(\hat{\mathbf{u}}_i - \mathbf{m}_i)^\top \mathbb{E}[\mathbf{m}_i - \mathbf{u}_i \mid \{\mathbf{Y}_{it}\}_{t=1}^{T_i}, \mathbf{B}, b_i, \sigma^2, \tau_u^2, \rho]. \end{aligned}$$

By definition of \mathbf{m}_i as the posterior mean,

$$\mathbb{E}[\mathbf{m}_i - \mathbf{u}_i \mid \{\mathbf{Y}_{it}\}_{t=1}^{T_i}, \mathbf{B}, b_i, \sigma^2, \tau_u^2, \rho] = \mathbf{0}.$$

Therefore,

$$R(\hat{\mathbf{u}}_i) = \|\hat{\mathbf{u}}_i - \mathbf{m}_i\|_2^2 + \mathbb{E}[\|\mathbf{m}_i - \mathbf{u}_i\|_2^2 \mid \{\mathbf{Y}_{it}\}_{t=1}^{T_i}, \mathbf{B}, b_i, \sigma^2, \tau_u^2, \rho].$$

The second term does not depend on $\hat{\mathbf{u}}_i$, and the first term is minimized uniquely at $\hat{\mathbf{u}}_i = \mathbf{m}_i$.

Hence the posterior mean \mathbf{m}_i is the Bayes estimator of \mathbf{u}_i under squared error loss. \square

Remark 4. This result gives a decision-theoretic interpretation to the proposed spatial deviation map. When the hierarchical model and the spatial covariance structure are correctly specified, the posterior mean \mathbf{m}_i is not merely a smoothed residual vector. It is the Bayes-optimal estimator of the individualized spatial deviation process under squared error loss. Since \mathbf{m}_i depends on $\mathbf{Q}(\rho)$ through the posterior covariance and precision structure, the spatial adjacency model directly enters the optimal estimator.

S3 Additional simulation implementation details

S3.1 Simulation design

The simulation study was designed to evaluate recovery of individualized deviation maps under varying spatial and longitudinal data structures. Each simulated dataset contained repeated measurements from multiple subjects observed across multiple brain regions. Data were generated directly from the hierarchical structure assumed by the proposed Bayesian longitudinal spatial normative model.

The simulations varied several characteristics relevant to longitudinal neuroimaging studies, including the strength of spatial dependence, nonlinear mean trajectories, irregular visit schedules, and missing follow-up. Six scenarios were considered in total:

1. baseline linear longitudinal structure,

2. moderate spatial dependence,
3. strong spatial dependence,
4. variable visit schedules,
5. missing longitudinal follow-up,
6. nonlinear mean trajectories.

For each simulated dataset, individualized abnormality maps were generated through latent subject-specific spatial deviation vectors. The same covariate structure and region-level adjacency assumptions were then used during model fitting.

S3.2 Construction of the spatial adjacency matrix

The spatial precision matrix was constructed from a region-level adjacency matrix

$$\mathbf{W}.$$

The matrix encoded neighborhood relationships between anatomically related regions. The diagonal degree matrix was defined as

$$D_{rr} = \sum_{r'} W_{rr'}.$$

The precision matrix used throughout the simulations was

$$Q(\rho) = D - \rho \mathbf{W},$$

where ρ controlled the strength of spatial dependence.

To ensure numerical stability and positive definiteness during posterior computation, a small diagonal ridge term was added when necessary. Different simulation scenarios used different values of ρ to represent weak, moderate, and strong anatomical dependence.

S3.3 Simulation performance metrics

Model performance was evaluated using both estimation accuracy and calibration criteria. Accuracy metrics included mean bias, mean squared error, and deviation-map mean squared error. The deviation-map mean squared error was used as the primary measure of individualized abnormality recovery because the principal inferential target of the proposed framework is the latent subject-specific deviation map.

Calibration metrics were based on the standardized deviation scores produced by each fitted model. Specifically, the simulations evaluated:

$$\mathbb{E}(Z), \quad \text{Var}(Z), \quad \Pr(|Z| > 1.96).$$

Well-calibrated normative models should produce approximately standard normal deviation scores under correct specification. Deviations from these targets indicate underestimation or overestimation of predictive uncertainty.

S4 Additional simulation results

The primary simulation summaries are reported in Tables 1–2 and Figures 1–2 of the main manuscript. Additional simulation diagnostics examined during model validation did not materially alter the reported findings and are therefore not presented separately.

Across simulation replicates, Bayesian model fitting remained stable, with representative fitted models exhibiting satisfactory convergence behavior, no divergent transitions, and \hat{R} values close to 1 across monitored parameters. Calibration summaries further showed that standardized deviation scores remained close to their target reference behavior across the simulated settings.

S5 Extended real-data analysis

S5.1 OASIS-3 structural neuroimaging data

The real-data application used longitudinal structural neuroimaging measurements from the OASIS-3 study (LaMontagne et al. 2019). OASIS-3 is a longitudinal neuroimaging, clinical, cognitive, and biomarker dataset designed to support studies of healthy aging and Alzheimer-type neurodegeneration. The dataset includes repeated MRI observations collected across multiple visits together with demographic and clinical information.

The present analysis focused on FreeSurfer-derived cortical thickness and subcortical volume measures. Structural measurements were merged with visit-level demographic and clinical variables and converted into long format so that each row represented a subject-region-visit combination.

Subjects were retained if they had at least two MRI visits after preprocessing and quality-control procedures. Observations with missing regional measurements, missing age information, or incomplete covariate data were excluded prior to model fitting.

S5.2 Regional measures and covariates

The analysis focused on cortical and subcortical regions commonly implicated in aging and neurodegenerative disease progression. These included bilateral hippocampus, amygdala, entorhinal cortex, parahippocampal cortex, temporal pole, inferior temporal cortex, middle temporal cortex, posterior cingulate cortex, and precuneus.

Regional measures were standardized within region before modeling:

$$Y_{itr}^{\text{std}} = \frac{Y_{itr} - \bar{Y}_r}{s_r},$$

where \bar{Y}_r and s_r denote the sample mean and sample standard deviation for region r . Standardization

allowed cortical thickness and subcortical volume measurements to be analyzed jointly on a comparable scale.

Age at MRI visit was standardized and included as the primary longitudinal covariate. FreeSurfer processing version was additionally included as a categorical adjustment variable to account for possible processing-version related variation in structural measurements.

S5.3 Real-data model specification

Three models were compared in the OASIS-3 application:

1. an independent cross-sectional regional model,
2. a longitudinal non-spatial mixed-effects model,
3. the proposed Bayesian subject-specific spatial model.

The proposed Bayesian model was

$$Y_{itr} = \alpha_r + \beta_r A_{it} + \gamma_{v[it]} + b_i + u_{ir} + \varepsilon_{itr},$$

where A_{it} denotes standardized age at visit and $\gamma_{v[it]}$ denotes the FreeSurfer-version effect.

The spatial adjacency structure connected anatomically related regions and bilateral homologous regions. Medial temporal, lateral temporal, and posterior cortical regions were additionally grouped into broader anatomical families to induce biologically plausible spatial borrowing across neighboring structures.

S5.4 Posterior computation and convergence assessment

The Bayesian model was implemented in Stan using the `cmdstanr` interface (Carpenter et al. 2017).

Four Markov chains were run with 1,000 warmup iterations and 1,000 post-warmup sampling

iterations per chain. The target acceptance probability was set to 0.99 and the maximum tree depth was set to 13.

Convergence was evaluated using traceplots, the potential scale reduction statistic \hat{R} , and effective sample size summaries. Posterior summaries for the key variance parameters were:

$$\sigma = 0.491, \quad \sigma_b = 0.517, \quad \tau_u = 0.928, \quad \sigma_{\text{version}} = 0.305.$$

All key parameters exhibited satisfactory convergence behavior with \hat{R} values close to one and adequate effective sample sizes.

S5.5 Additional real-data findings

The Bayesian subject-specific spatial model produced substantially improved individualized fit relative to the benchmark models. The residual standard deviation decreased from 0.926 under the independent cross-sectional model and 0.774 under the longitudinal non-spatial model to 0.423 under the Bayesian spatial model. The proposed framework also produced lower mean absolute deviation and improved calibration of standardized deviation scores.

Regional summaries identified the temporal pole, entorhinal cortex, inferior temporal cortex, posterior cingulate cortex, and amygdala as regions exhibiting the greatest burden of extreme deviations. These findings are biologically consistent with regions commonly implicated in aging and Alzheimer-type neurodegenerative processes.

Subject-level analyses further demonstrated substantial heterogeneity in individualized abnormality burden across participants. Several subjects exhibited persistent extreme deviation trajectories across repeated visits despite relatively preserved cognitive scores, illustrating the ability of the proposed framework to identify individualized structural abnormality patterns beyond simple group-average summaries.

S5.6 Supplementary real-data figures

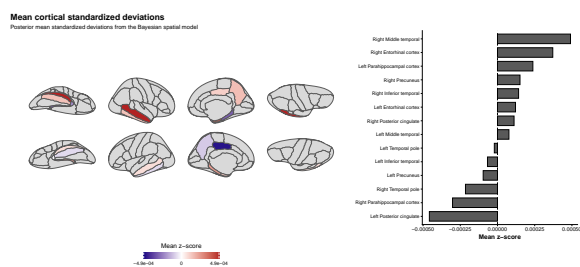


Figure S1: Mean cortical standardized deviations from the Bayesian subject-specific spatial model. This figure complements the main cortical extreme-deviation map by displaying posterior mean deviations rather than tail probabilities.

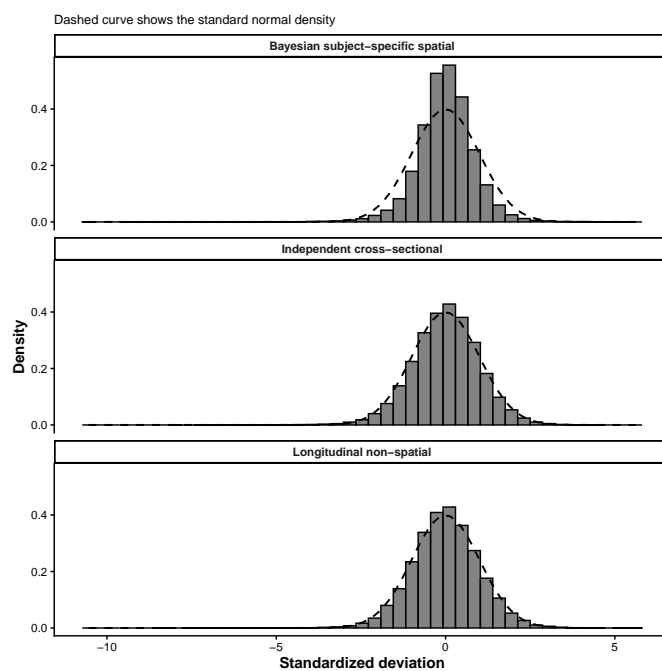


Figure S2: Calibration histograms for standardized deviation scores across the three OASIS-3 models. The dashed curve represents the standard normal density.

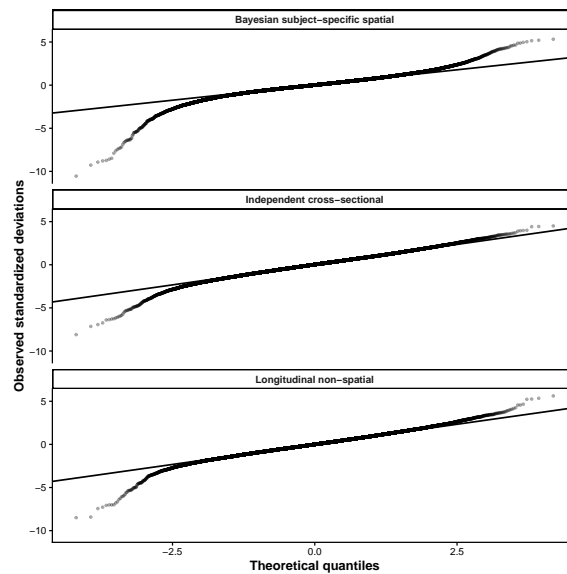


Figure S3: Normal QQ plots for standardized deviation scores across the independent cross-sectional, longitudinal non-spatial, and Bayesian subject-specific spatial models.

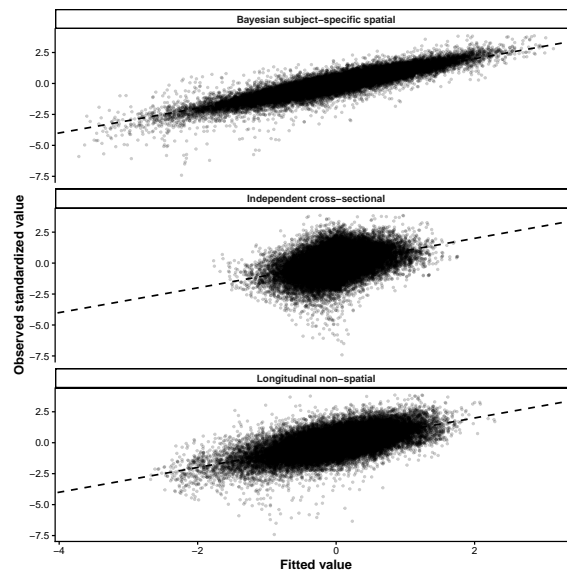


Figure S4: Observed versus fitted standardized structural measurements across the three OASIS-3 models. Points closer to the diagonal indicate better agreement between fitted and observed standardized values.

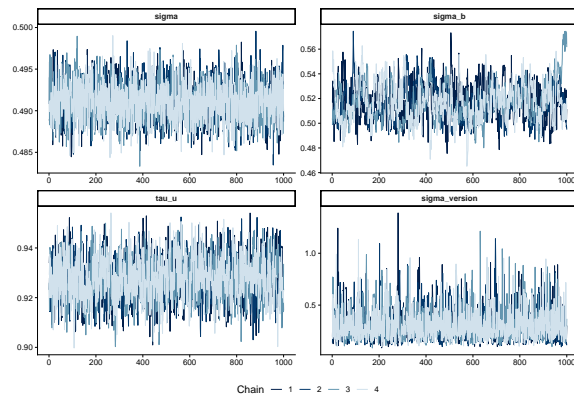


Figure S5: MCMC traceplots for key posterior scale parameters in the Bayesian subject-specific spatial model. Chains showed stable mixing around common posterior ranges.

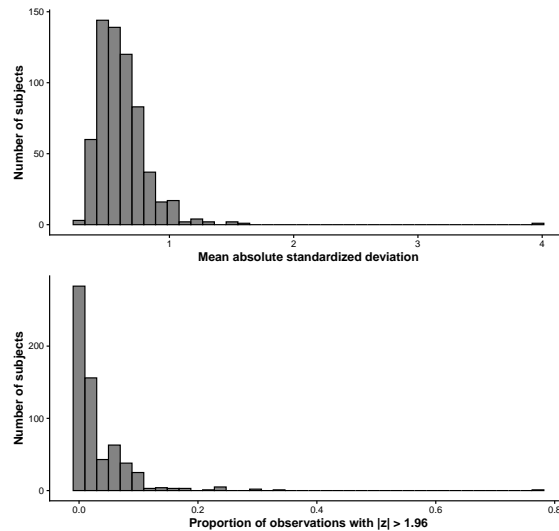


Figure S6: Distribution of subject-level abnormality burden in the OASIS-3 application, summarized by mean absolute standardized deviation and the proportion of observations exceeding $|Z| > 1.96$.

S5.7 Sensitivity analyses

Multiple sensitivity analyses were considered to evaluate the robustness of the proposed framework. These included alternative specifications of the spatial adjacency matrix, exclusion of subjects with unusually large deviation burdens, and comparison with models excluding spatial dependence.

Table S1: Posterior summaries for key variance and scale parameters in the OASIS-3 Bayesian subject-specific spatial model.

Parameter	Mean	Median	SD	5%	95%	\widehat{R}	Bulk ESS
σ	0.4911	0.4911	0.0023	0.4875	0.4949	1.0024	2741.8
σ_b	0.5174	0.5164	0.0148	0.4952	0.5425	1.0077	226.0
τ_u	0.9277	0.9277	0.0085	0.9140	0.9416	1.0025	1262.2
σ_{version}	0.3047	0.2669	0.1472	0.1405	0.5874	0.9995	1612.3

Table S2: Selected subjects used for the illustrative low-deviation and high-abnormality case-study profiles.

Subject	Observations	Visits	Mean $ Z $	Max $ Z $	Extreme proportion	Mean MMSE
OAS30765	57	3	0.3481	1.2055	0.0000	26.33
OAS30303	57	3	3.9663	10.5478	0.7719	29.67

The principal findings remained stable across these analyses. In particular, the Bayesian spatial model consistently produced lower deviation-map reconstruction error and more stable individualized abnormality estimates than the benchmark models. Regional abnormality patterns remained concentrated within temporo limbic and posterior cortical regions across alternative specifications.

Table S3: Regions with the largest extreme-deviation burden in the OASIS-3 application.

Region	Observations	Mean Z	SD Z	$\Pr(Z > 1.96)$
Right temporal pole thickness	1902	-0.0002	1.1064	0.0778

Region	Observations	Mean Z	SD Z	$\Pr(Z > 1.96)$
Left temporal pole thickness	1902	0.0000	1.0881	0.0705
Right entorhinal thickness	1902	0.0004	1.0196	0.0547
Left entorhinal thickness	1902	0.0001	0.9713	0.0515
Right inferior temporal thickness	1902	0.0001	0.9305	0.0410
Left inferior temporal thickness	1902	-0.0001	0.9271	0.0379
Left posterior cingulate thickness	1902	-0.0005	1.0108	0.0352
Left amygdala volume	1902	0.0003	0.8713	0.0342
Right amygdala volume	1902	-0.0002	0.9169	0.0331
Left middle temporal thickness	1902	0.0001	0.8350	0.0289

S6 Computational details

All analyses were conducted in R using `cmdstanr`, `posterior`, `ggplot2`, `dplyr`, `Matrix`, and `brms`. Bayesian posterior inference was performed using Hamiltonian Monte Carlo implemented in Stan.

The primary computational settings included:

- four Markov chains,
- 1,000 warmup iterations per chain,
- 1,000 post-warmup sampling iterations per chain,
- target acceptance probability of 0.99,
- maximum tree depth of 13.

Posterior convergence was assessed using traceplots, effective sample size summaries, and \hat{R}

statistics. Posterior summaries were computed using the `posterior` package.

The complete analysis pipeline, including preprocessing, simulation generation, Bayesian model fitting, and visualization, was implemented using reproducible scripts.

References

- Bakkour, A., Morris, J. C. & Dickerson, B. C. (2009), ‘The cortical signature of prodromal ad: regional thinning predicts mild ad dementia’, *Neurology* **72**(12), 1048–1055.
- Banerjee, S., Carlin, B. P. & Gelfand, A. E. (2003), *Hierarchical modeling and analysis for spatial data*, Chapman and Hall/CRC.
- Bayer, J. M., Dinga, R., Kia, S. M., Kottaram, A. R., Wolfers, T., Lv, J., Zalesky, A., Schmaal, L. & Marquand, A. (2022), ‘Accommodating site variation in neuroimaging data using normative and hierarchical bayesian models’, *NeuroImage* **264**, 119699.
- Besag, J. (1974), ‘Spatial interaction and the statistical analysis of lattice systems’, *Journal of the Royal Statistical Society: Series B (Methodological)* **36**(2), 192–225.
- Bethlehem, R. A., Seidlitz, J., White, S. R., Vogel, J. W., Anderson, K. M., Adamson, C., Adler, S., Alexopoulos, G. S., Anagnostou, E., Areces-Gonzalez, A. et al. (2022), ‘Brain charts for the human lifespan’, *Nature* **604**(7906), 525–533.
- Bucková, B. R., Frazza, C., Reháč, R., Kolenič, M., Beckmann, C. F., Španiel, F., Marquand, A. F. & Hlinka, J. (2025), ‘Using normative models pre-trained on cross-sectional data to evaluate intra-individual longitudinal changes in neuroimaging data’, *Elife* **13**, RP95823.
- Carpenter, B., Gelman, A., Hoffman, M. D., Lee, D., Goodrich, B., Betancourt, M., Brubaker, M., Guo, J., Li, P. & Riddell, A. (2017), ‘Stan: A probabilistic programming language’, *Journal of statistical software* **76**, 1–32.

- De Oliveira, V. (2012), 'Bayesian analysis of conditional autoregressive models', *Annals of the Institute of Statistical Mathematics* **64**(1), 107–133.
- Dickerson, B. C., Bakkour, A., Salat, D. H., Feczko, E., Pacheco, J., Greve, D. N., Grodstein, F., Wright, C. I., Blacker, D., Rosas, H. D. et al. (2009), 'The cortical signature of alzheimer's disease: regionally specific cortical thinning relates to symptom severity in very mild to mild ad dementia and is detectable in asymptomatic amyloid-positive individuals', *Cerebral cortex* **19**(3), 497–510.
- Fischl, B., Van Der Kouwe, A., Destrieux, C., Halgren, E., Ségonne, F., Salat, D. H., Busa, E., Seidman, L. J., Goldstein, J., Kennedy, D. et al. (2004), 'Automatically parcellating the human cerebral cortex', *Cerebral cortex* **14**(1), 11–22.
- Fraza, C. J., Dinga, R., Beckmann, C. F. & Marquand, A. F. (2021), 'Warped bayesian linear regression for normative modelling of big data', *NeuroImage* **245**, 118715.
- Gaiser, C., Berthet, P., Kia, S., Frens, M., Beckmann, C., Muetzel, R. & Marquand, A. F. (2024), 'Estimating cortical thickness trajectories in children across different scanners using transfer learning from normative models', *Human Brain Mapping* **45**(2), e26565.
- Gelman, A. (2006), 'Prior distributions for variance parameters in hierarchical models (comment on article by browne and draper)', pp. 515–534.
- Huertas, I., Oldehinkel, M., van Oort, E. S., Garcia-Solis, D., Mir, P., Beckmann, C. F. & Marquand, A. F. (2017), 'A bayesian spatial model for neuroimaging data based on biologically informed basis functions', *NeuroImage* **161**, 134–148.
- Kia, S. M., Huijsdens, H., Dinga, R., Wolfers, T., Mennes, M., Andreassen, O. A., Westlye, L. T., Beckmann, C. F. & Marquand, A. F. (2020), Hierarchical bayesian regression for multi-site

- normative modeling of neuroimaging data, *in* ‘International Conference on Medical Image Computing and Computer-Assisted Intervention’, Springer, pp. 699–709.
- Laird, N. M. & Ware, J. H. (1982), ‘Random-effects models for longitudinal data’, *Biometrics* pp. 963–974.
- LaMontagne, P. J., Benzinger, T. L., Morris, J. C., Keefe, S., Hornbeck, R., Xiong, C., Grant, E., Hassenstab, J., Moulder, K., Vlassenko, A. G. et al. (2019), ‘Oasis-3: longitudinal neuroimaging, clinical, and cognitive dataset for normal aging and alzheimer disease’, *medrxiv* pp. 2019–12.
- Marquand, A. F., Kia, S. M., Zabihi, M., Wolfers, T., Buitelaar, J. K. & Beckmann, C. F. (2019), ‘Conceptualizing mental disorders as deviations from normative functioning’, *Molecular psychiatry* **24**(10), 1415–1424.
- Marquand, A. F., Rezek, I., Buitelaar, J. & Beckmann, C. F. (2016), ‘Understanding heterogeneity in clinical cohorts using normative models: beyond case-control studies’, *Biological psychiatry* **80**(7), 552–561.
- Mejia, A. F., Koppelmans, V., Jelsone-Swain, L., Kalra, S. & Welsh, R. C. (2022), ‘Longitudinal surface-based spatial bayesian glm reveals complex trajectories of motor neurodegeneration in als’, *NeuroImage* **255**, 119180.
- Polson, N. G. & Scott, J. G. (2012), ‘On the half-cauchy prior for a global scale parameter’.
- Rue, H. & Held, L. (2005), *Gaussian Markov random fields: theory and applications*, Chapman and Hall/CRC.
- Rutherford, S., Barkema, P., Tso, I. F., Sripada, C., Beckmann, C. F., Ruhe, H. G. & Marquand, A. F. (2022), ‘Evidence for embracing normative modeling’, *bioRxiv* pp. 2022–11.
- Rutherford, S., Kia, S. M., Wolfers, T., Frazza, C., Zabihi, M., Dinga, R., Berthet, P., Worker, A.,

- Verdi, S., Ruhe, H. G. et al. (2022), ‘The normative modeling framework for computational psychiatry’, *Nature protocols* **17**(7), 1711–1734.
- Sina, M. L., Di Biase, M. A., Zhang, C., Tian, F., Zhang, S., Yan, H., Xue, A., Chong, J. S. X., Dehestani, N., Ng, E. K.-K. et al. (2025), ‘Spectral normative modeling of brain structure’, *medRxiv* pp. 2025–01.
- Verdi, S., Kia, S. M., Yong, K. X., Tosun, D., Schott, J. M., Marquand, A. F. & Cole, J. H. (2023), ‘Revealing individual neuroanatomical heterogeneity in alzheimer disease using neuroanatomical normative modeling’, *Neurology* **100**(24), e2442–e2453.
- Verdi, S., Marquand, A. F., Schott, J. M. & Cole, J. H. (2021), ‘Beyond the average patient: how neuroimaging models can address heterogeneity in dementia’, *Brain* **144**(10), 2946–2953.
- Verdi, S., Rutherford, S., Frazza, C., Tosun, D., Altmann, A., Raket, L. L., Schott, J. M., Marquand, A. F., Cole, J. H. & Initiative, A. D. N. (2024), ‘Personalizing progressive changes to brain structure in alzheimer’s disease using normative modeling’, *Alzheimer’s & Dementia* **20**(10), 6998–7012.